

ADVECTION SCHEMES FOR CAPTURING RELATIVISTIC SHOCKS WITH HIGH LORENZ FACTORS

HUJEIRAT, A.A.^{1,2} AND FEHLMANN, S.²
Draft version November 19, 2018

ABSTRACT

Jet-plasmas emanating from the vicinity of relativistic objects and in gamma-ray bursts have been observed to propagate with Lorentz factors laying in the range between one and several hundreds. On the other hand, the numerical studies of such flows have been focussed so far mainly on the lowest possible range of Lorentz factors Γ , specifically, on the regime $1 \leq \Gamma \leq 5$. Therefore, relativistic flows with high Γ -factors have poorly studied, as most numerical methods are found to encounter severe numerical difficulties or even become numerically unstable for $\Gamma \gg 1$.

In this paper we present an implicit numerical advection scheme for modeling the propagation of relativistic plasmas with shocks, discuss its consistency with respect to both the internal and total energy formulation in general relativity. Using the total energy formulation, the scheme is found to be viable for modeling moving shocks with moderate Lorentz factors, though with relatively small Courant numbers. In the limit of high Lorentz factors, the internal energy formulation in combination with a fine-tuned artificial viscosity is much more robust and efficient. We confirm our conclusions by performing test calculations and compare the results with analytical solutions of the relativistic shock tube problem. The aim of the present modification is to enhance the robustness of the general relativistic implicit radiative MHD solver: GR-I-RMHD (<http://www1.iwr.uni-heidelberg.de/groups/compastro/home/gr-i-mhd-solver>) and extend its range of applications into the high Γ -regime.

Subject headings: Relativity: numerical, — Hydrodynamics: relativistic, advection schemes — Numerical methods: shock capturing, numerical accuracy — fluids: Euler and Navier-Stokes equations

1. INTRODUCTION

Plasmas moving at relativistic speeds have been observed in diverse astrophysical phenomena, such as in supernova explosions, in jets emanating from around neutron stars, in microquasars and in active galactic nuclei (see Livio 2004; Marscher 2006; Fender et al. 2007, and the references therein). The bulk Lorentz factor, Γ , of the observed jet-plasmas, in most cases, has been found to increase with the mass of the central relativistic object. Jets ejected by neutron stars generally propagate with Γ_{NS} between 1 and 3, in microquasars $\Gamma_{\mu QSO}$ is between 1 and 4 whereas in AGNs/QSOs Γ_{AGN} is between 5 and 10. Gamma-ray bursts are considered to be an extreme case, as the Lorentz factors here is considered to be of the order of several hundreds (e.g., Piran 2006).

Jet-plasmas considered to decelerate via self-interaction or interaction with the surrounding media in the form of shocks and eventually become efficient sources for the production of the observed high energy gamma-rays and probably for the energetic cosmic rays (Sikora 1994).

Modeling the formation of relativistic shock by means of HD and MHD simulation has been the focus of numerous studies during the the last two decades (Hawley et al. 1984b; Alay et al. 1999; Font et al. 2000; Hujeirat 2003; Marti and Müller 2003; De Villiers, Hawley 2003; Gammie et al. 2003; Anninos, Fragile 2003; Komissarov 2004; Del Zanna et al. 2007; Mignone et al. 2007; Hujeirat et al. 2008, see also the references therein).

These studies have enriched the field of computational astrophysics with numerical techniques and useful strategies for accurate capturing of relativistic shock fronts us-

ing both the internal and total energy formulation (e.g., De Villiers, Hawley 2003; Mignone et al. 2007). Nevertheless, most of these methods encounter numerical difficulties when modeling relativistic flows with high Lorentz factors, i.e., $\Gamma \geq 5$. In the literature, results of relativistic shock tube problems with merely moderate Γ -factors have been presented (see Hawley et al. 1984; Alay et al. 1999; Zhang 2006; Mignone et al. 2007, and the references therein).

The numerical difficulties associated with modeling flows with high Lorentz factors originate from the small initial velocity errors in the momentum equations. These errors correlate with Γ^2 , hence they are highly non-linear and may be strongly magnified as the time-iteration proceeds. This may give rise to a significant over/under estimation of the other variables. Recipes, such as further reducing the grid spacing and/or the time-step size may lead to a stagnation of the solution procedure, in particular if the method used is conditionally stable.

On the other hand, only a limited effort has been made to develop time-implicit numerical solvers for simulating relativistic flows in astrophysics. The main reason therefore is that most astrophysical flows are intrinsically time-dependent with strong spatial variations, which implies that the numerical scheme must be highly accurate in time and space. However, the leading temporal errors generally scale as the time step size $\sim \delta t$ or the power of it. Thus δt must be sufficiently small and in most cases, it must be even smaller than the sound-crossing time between the boundaries of a single finite volume cell. This is equivalent to require that the Courant number be smaller than unity and therefore ending up with the stability requirement of conditionally stable methods. In this regime explicit methods are much more efficient than their implicit counterparts, as implicit methods require

¹ IWR - Interdisciplinary Center for Scientific Computing, Heidelberg University, INF 368, 69120 Heidelberg, Germany

² Departement Physik, University of Basel, Switzerland

the inversion of a matrix A_{imp} (e.g. Eq. 1) in order to solve the set of linear equations $Ax = b$ that corresponds to the linearized hydrodynamical equations in the finite space.

$$A_{imp} \sim \begin{pmatrix} \frac{a}{\epsilon} & \epsilon & \epsilon & \epsilon \\ \epsilon & \frac{a}{\epsilon} & \epsilon & \epsilon \\ & & \ddots & \\ \epsilon & \epsilon & \epsilon & \frac{a}{\epsilon} \end{pmatrix} \quad (1)$$

On the other hand, it can be easily verified that one may obtain almost the same results when A_{imp} is replaced by $A_{exp} = \frac{a}{\epsilon} I$, where I is the identity matrix³. A_{exp} is the pre-conditioner generally used by explicit methods for solving the same set of equations, thereby avoiding the formidable arithmetic operations associated with the inversion procedure of A_{imp} .

However, most astrophysical flows are by nature dissipative, radiative and magnetic-diffusive and therefore are well-described by the the generalized Navier-Stokes (-NS) rather than the Euler equations. Such physically non-ideal effects generally do not operate uniformly in the domain of calculations and they may occur also on longer or shorter time scales than the dynamical one. As a consequence, the NS-solvers should not only be unconditionally stable, but they must be sufficiently robust to treat limiting cases such as Euler type-flows, event hough their efficiency for these specific cases might be too low compared to explicit methods.

, hence the purpose of the present paper. Moreover, we show that our time-implicit method in combination with a modified third order MUSCL advection scheme is capable of modeling shocks propagating with Lorentz factors $\Gamma \geq 10$ with time step sizes corresponding to Courant numbers larger than 100.

In Sec. 2 we describe the hydrodynamical equations solved in the present study. The solution method relies on using the 3D axi-symmetric general relativistic implicit radiative MHD solver (henceforth GR-I-RMHD), which has been described in details in a series of articles (e.g., Hujeirat et al. 2008; Hujeirat & Thielemann. 2009). In Sec. (3) we just focus on several new aspects of the advection scheme. The results of the verification tests are presented in Sec. (4) and end up with Sec. (5), where the results of the present study are summarized.

2. THE 1D GENERAL RELATIVISTIC HYDRODYNAMICAL EQUATIONS

In the present study we consider the set of Euler equations in one-dimension and in flat spacetime:

$$\begin{aligned} \partial_t D + \nabla_r \cdot (D V^r) &= 0 \\ \partial_t M_r + \nabla_r \cdot (M_r V^r) &= -\partial_r P \\ \partial_t \mathcal{E}^{\text{tot}} + \nabla_r \cdot ([\mathcal{E}^{\text{tot}} + P] V^r) &= 0, \end{aligned} \quad (2)$$

where $\nabla_r \cdot (\doteq \frac{1}{\sqrt{-g}} \partial_r \sqrt{-g})$, is the radial component of the divergence operator in flat space with the signature $(-, +, +, +)$ and „g“ is the determinant of the coefficient matrix corresponding to the metric. $D (\doteq \rho u^t)$ is the relativistic density, M_r is the radial component of the 4-momentum: $M_\mu \doteq \bar{D} u_\mu$, where u_μ is the 4-velocity, u^t

³ The similarity between the real Jacobian \mathcal{J} and the matrices A_{imp} and A_{exp} applies for a sufficiently small δt .

is the time-like velocity⁴, $V^r (= u^r/u^t)$ is the transport velocity, $\bar{D} \doteq Dh$, and “h” is the relativistic enthalpy $h = c^2 + \epsilon + P/\rho$. $\mathcal{E}^{\text{tot}} = (u^t)^2 \rho h - P$ is the total energy which is the sum of kinetic and thermal energies of the gas. “P” is the pressure of ideal gas: $P = (\gamma - 1)\rho\epsilon$, ϵ and γ denote the internal energy and the corresponding adiabatic index, respectively.

In the rest of this paper, we will set $c=1$.

The reader is referred to Sec. (2) of Hujeirat et al. (2008), where the general relativistic hydrodynamical equations and their derivations in the Boyer-Lindquist coordinates are described. However, we continue to use these coordinates, though in the limit of flat space.

In the case that the mechanical energy is conserved, then the total energy reduces to an evolutionary equation for the internal energy:

$$\partial_t \mathcal{E}^d + \nabla_r \cdot (\mathcal{E}^d V^r) = -(\gamma - 1) \frac{\mathcal{E}^d}{u^t} [\partial_t u^t + \nabla_r \cdot (u^t V^r)] \quad (3)$$

where $\mathcal{E}^d = u^t P / (\gamma - 1)$.

Furthermore, there is a remarkable similarity of how Eq. (3) deals with \mathcal{E}^d and u^t . Taking this similarity into account, the equation can be re-formulated to have the following form:

$$\partial_t \bar{\mathcal{E}}^d + \nabla_r \cdot (\bar{\mathcal{E}}^d V^r) = -\gamma D (\nabla_r \cdot V^r), \quad (4)$$

where $\bar{\mathcal{E}}^d = D \log[\mathcal{E}^d (u^t)^{\gamma-1}]$.

In Equation (2), the energy equation describes the time-evolution of the total energy \mathcal{E}^{tot} . Our numerical solution method relies first on selecting the primary variables and calculating their corresponding entries in the Jacobian. We then iterate to recover the correct contributions of the depending variables, such as the transport velocity and pressure. Therefore, the advection operator can be decomposed into two parts as follows:

$$\partial_t \mathcal{E}^{\text{tot}} + \nabla_r \cdot (\mathcal{E}^{\text{tot}} V^r) = \nabla_r \cdot (P V^r). \quad (5)$$

This equation is solved as follows: Solve for \mathcal{E}^{tot} using the pressure from the last iteration level. Once \mathcal{E}^{tot} and “D” are known, we may proceed to update the pressure as follows:

$$P = \frac{\mathcal{E}^{\text{tot}} - u^t D}{\frac{\gamma}{\gamma-1} (u^t)^2 - 1}. \quad (6)$$

This value of “P” is then inserted again into the RHS of Equation (5) to compute a corrected value for \mathcal{E}^{tot} .

The effect of iteration can be reduced on the cost of using pressure values from the last time step using the following alternative formulation:

$$\partial_t \bar{\mathcal{E}}^{\text{tot}} + \nabla_r \cdot (\bar{\mathcal{E}}^{\text{tot}} V^r) = \partial_t P, \quad (7)$$

where $\bar{\mathcal{E}}^{\text{tot}} = (u^t)^2 \rho h$.

Thus, once $\bar{\mathcal{E}}^{\text{tot}}$ is found, the pressure can be computed from the known conservative variables as follows:

$$P = \frac{\gamma - 1}{\gamma} \frac{\bar{\mathcal{E}}^{\text{tot}} - u^t D}{(u^t)^2}. \quad (8)$$

⁴ u^t is also the general relativistic Lorentz factor, which reduces to the classical Γ in flat space.

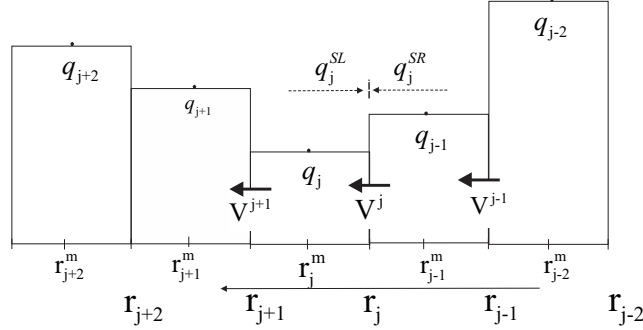


Figure 1. A schematic description of several finite volume cells, their boundaries and the location of the scalar quantities "q" and the velocities.

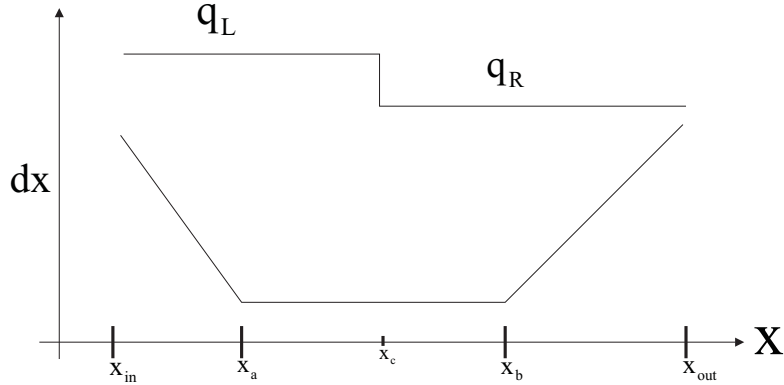


Figure 2. Grid spacing versus position. The interval of calculations is a priori divided into two regions: $[x_a \leq x \leq x_b]$, where the physical variables are expected to change and the sub-intervals $x \leq x_a$ and $x \geq x_b$, where the physical variables do not change. Therefore the grid spacing in the interval $[x_a \leq x \leq x_b]$ is set to be uniform, whereas in the rest intervals only several non-uniform grid-points have been used to save computer time. The initial conditions for the first test problem read: for $x \leq x_c$: $P_L = 40/3$, $\rho_L = 10$ and for $x > x_c$: $P_R = (2/3) \times 10^{-6}$ and $\rho_R = 1$.

On the other hand, using the internal energy formulation for modeling moving shocks requires the inclusion of an artificial viscosity for calculating their fronts accurately. This modification is necessary in order to recover the loss of heat generally produced through the conversion of kinetic energy into internal energy at the shock fronts.

In this case, the RHS of Equation (3) should be modified to include the artificial heating term:

$$Q_{art}^+ = \eta_{art} (\partial_\mu u^t V^\mu)^2, \quad \mu = 0, 1, 2, 3 \quad (9)$$

where η_{art} is the artificial viscosity coefficient.

The inclusion of Q_{art}^+ implies an enhancement of the effective pressure. Therefore, the thermodynamical pressure, and also the enthalpy, should be modified to include an artificial pressure of the form:

$$P_{tot} = P + P_{art} = P + \eta_{art} \partial_\mu (u^t V^\mu). \quad (10)$$

Note that the artificial pressure enters the momentum equation in the form of ∇P_{art} , which scales as $\sim \Delta(\eta_{art} V)$. This is equivalent to activating a second order viscous operator at the shock fronts, whose effect is then to transport information from the downstream to the upstream regions, so to enhance the stability of the transport scheme in such critical transitions.

2.1. Determining the Lorentz factor

Our test calculations showed that the Lorentz factor can be best determined from the normalization condition, in which both the conservative variables and transport velocities are involved. To clarify this point, the normalization condition reads:

$$\begin{aligned} -1 &= u^\mu u_\mu \\ &= (u^t V^\mu) \left(\frac{M_\mu}{D} \right) \\ &= \frac{u^t}{D} [M_t + V^r M_r + V^\theta M_\theta + V^\varphi M_\varphi] \\ &= \frac{u^t}{D} \left[\left\{ \frac{M^t - g^{t\varphi} M_\varphi}{g^{tt}} \right\} + V^\theta M_\theta + V^\varphi M_\varphi \right] \\ &= \frac{u^t}{D} \left[\left(\frac{\bar{D} u^t}{g^{tt}} \right) + V^\theta M_\theta + \left(V^\varphi - \frac{g^{t\varphi}}{g^{tt}} \right) M_\varphi \right], \end{aligned} \quad (11)$$

where the velocities are in light speed units, $\bar{D} = \rho h u^t$, which can be directly determined from the continuity and the energy equations, V^μ is the transport velocity and $g^{\mu\nu}$ are the elements of the metric.

The final form of Eq. (11) is the quadratic equation: $A (u^t)^2 + B u^t + C = 0$, where A, B and C are parameters independent of u^t . Thus, the Lorentz factors can be determined from this equation completely.

We note that since the state of the conservative variables D , M_μ , \mathcal{E}^d depends strongly on the transport velocity V^μ , it is therefore necessary to consider V^μ when computing the Lorentz factor u^t as described in Eq. (11).

3. THE NUMERICAL METHOD: ADVECTION SCHEME FOR HIGH LORENTZ FACTORS

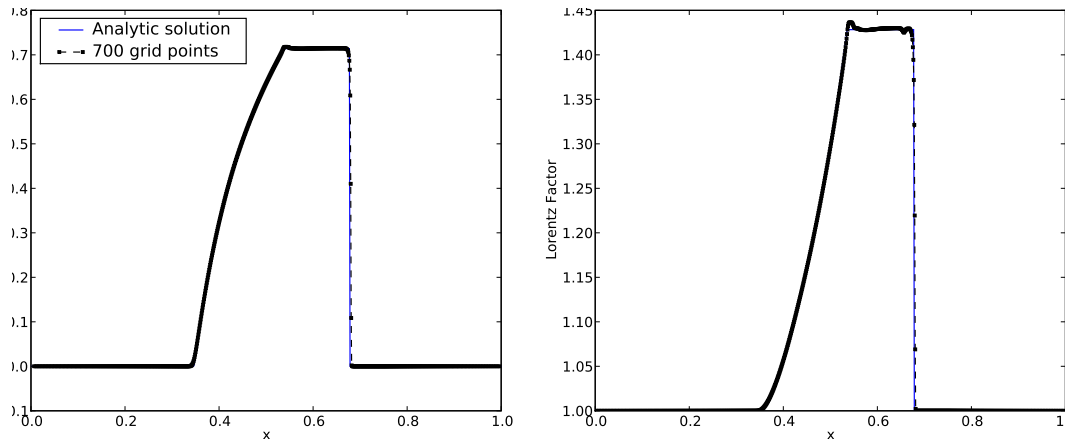


Figure 3. The profiles of the velocity V (left) and the Lorentz factor u^t (right, dashed line connecting squares) overplotted on the corresponding analytical solutions (continuous blue lines) after $\tau = 0.2$. The numerical solutions have been obtained using the total energy formulation (TEF). The initial pressure was taken to be $P_L = 40/3$, $\rho_L = 10$, $P_R = (2/3) \times 10^{-6}$, $\rho_R = 1$. We use 700 non-uniformly distributed grid points, $CFL=0.4$ and perform two global iterations in each time step. The advection scheme employed here is of third order spatial and second order temporal accuracy.

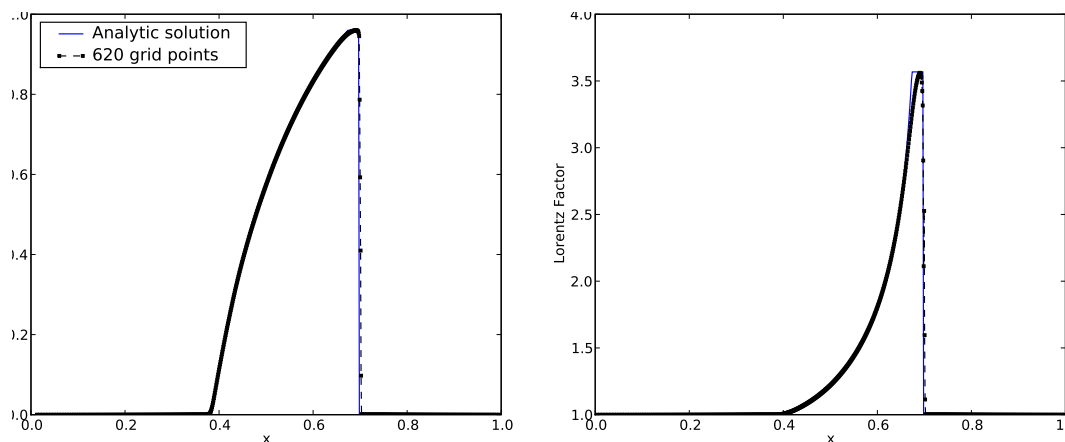


Figure 4. As in Fig (3), the profiles of V and u^t have been obtained using the TEF, an initial pressure $P_L = 10^2 P_{L0}$ and $CFL=0.4$. 620 non-uniformly distributed grid points have been used in combination with four global iterations per time step.

The advection scheme presented in Sec. (3.1) is incorporated and solved using the implicit general relativistic numerical MHD solver, GR-I-RMHD. This solver has been described in details in Hujeriat et al. (2008). For completeness, we briefly mention that GR-I-RMHD is a 3D axi-symmetric, time-implicit solver, which relies on using the powerful preconditioned defect-correction iterative strategy in combination with the nonlinear Newtonian iterative method. By preconditioning we mean constructing a matrix that is similar to the original Jacobian obtained by differentiating the equations with respect to the main unknown variables.

The advantages of implicit over explicit methods are prominent when quasi-stationary or time-independent flow configurations are sought. However, for strongly time-dependent flow features, such as moving shock and turbulence, explicit methods are much more efficient, provided that flow is almost ideal, i.e., non-reacting and non-dissipative. Towards enlarging the range of applications of GR-I-RMHD to include the regime of high Lorentz factors, the advection scheme presented in Sec. (3.1) has been incorporated and verification tests have been performed (see Sec. 4).

3.1. The third order advection scheme

Most time-implicit advection schemes generally rely on upwinding to stabilize the transport near critical fronts. Transport of quantities here can be mediated with CFL numbers larger than unity. Therefore, the advection scheme employed should be independent of the time step size. Indeed, the monotone upstream centered schemes for conservation laws, or simply the MUSCL schemes, obey these conditions (see Hirsch 1988, and the references therein). However, in order to model moving shocks with high Lorentz factors accurately, it is necessary to modify the scheme, so that the information-flow from the downstream to upstream regions should be further limited in accordance with the normalization condition, i.e., causality condition.

A classical advection scheme of the MUSCL-type gives the following interface values:

$$\begin{aligned} q_{j-1/2}^{SR} &= q_{j-1} - \frac{1}{4}[(1 + \kappa)\Delta q_{j-1} + (1 - \kappa)\Delta q_{j-2}] & : \text{if } V_j \leq 0 \\ q_{j-1/2}^{SL} &= q_j + \frac{1}{4}[(1 - \kappa)\Delta q_j + (1 + \kappa)\Delta q_{j+1}] & : \text{if } V_j > 0, \end{aligned} \quad (12)$$

where “q” is the transported physical quantity, κ is a

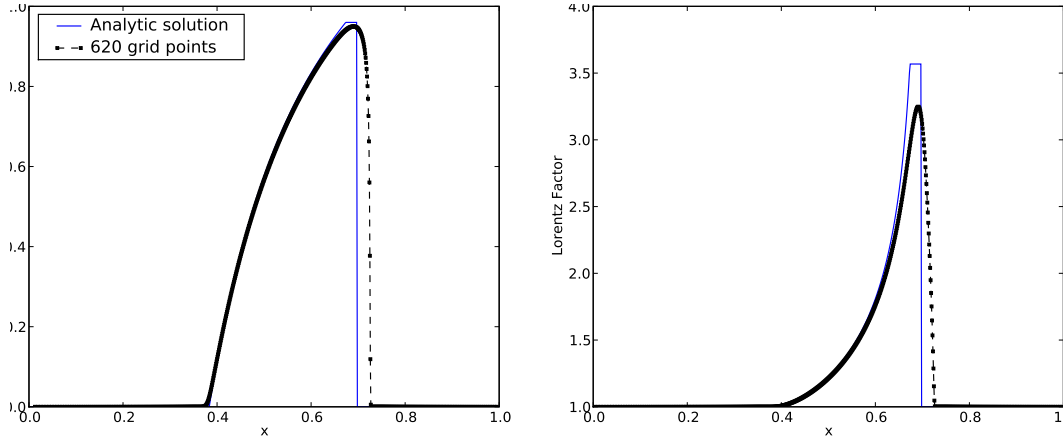


Figure 5. As in Fig (3), the profiles of V and u^t have been obtained using the TEF, an initial pressure $P_L = 10^2 P_{L0}$ and $CFL = 0.4$. An upwind advection scheme of first order spatial accuracy and two global iterations per time step have been used.

switch off/on parameter that specify the accuracy needed and $\Delta q_j = q_j - q_{j+1}$. Note that the scheme is of second order for $\kappa = -1, 0, 1$ and of third order for $\kappa = 1/3$.

In order to enable an accurate capturing of shock fronts propagating with high Lorentz factors on a non-uniform grid distribution, the following modifications have been performed:

$$\begin{aligned} \text{if } V_j \leq 0: & \quad q_j^{SR} = q_{j-1} - \frac{1}{4}[(1 - \sigma)\Delta q_j + (1 + \sigma)\Delta q_{j-1}], \\ & \quad \text{where } \sigma = 2\kappa (\Delta q_j^{RR} \cdot \Delta q_j^{OR}) / [(\Delta q_j^{RR})^2 + (\Delta q_j^{OR})^2 + \epsilon], \\ \text{if } V_j > 0: & \quad q_j^{SL} = q_j + \frac{1}{4}[(1 + \sigma)\Delta q_j + (1 - \sigma)\Delta q_{j+1}], \\ & \quad \text{where } \sigma = 2\kappa (\Delta q_j^{OL} \cdot \Delta q_j^{LL}) / [(\Delta q_j^{OL})^2 + (\Delta q_j^{LL})^2 + \epsilon], \end{aligned} \quad (13)$$

where

$$\begin{aligned} \Delta q_j^{RR} &= (x_{j-1}^m - x_j^m)(q_{j-2} - q_{j-1}) / (x_{j-2}^m - x_{j-1}^m) \\ \Delta q_j^{OR} &= (x_{j-2}^m - x_{j-1}^m)(q_{j-1} - q_j) / (x_{j-1}^m - x_j^m) \\ \Delta q_j^{OL} &= (x_j^m - x_{j+1}^m)(q_{j-1} - q_j) / (x_{j-1}^m - x_j^m) \\ \Delta q_j^{LL} &= (x_{j-1}^m - x_j^m)(q_j - q_{j+1}) / (x_j^m - x_{j+1}^m), \end{aligned} \quad (14)$$

and where ϵ is a small number set to avoid division by zero.

The accuracy of above modified scheme may be further increased by incorporating the Lagrangian Upwind Interpolation Scheme (LUIS). The LUIS strategy is based on by constructing a Lagrangian polynomial of third or fourth order whose main weight is shifted to the right or left, depending on the upwind direction. The final combined LUIS-MUSCL scheme reads as follows:

$$\begin{aligned} \text{if } V_j \leq 0: & \quad q_j^{SR} = \xi q_j^{SR} + (1 - \xi)Lq_j^{SR}, \\ \text{if } V_j > 0: & \quad q_j^{SL} = \xi q_j^{SL} + (1 - \xi)Lq_j^{SL}, \end{aligned} \quad (15)$$

where ξ is an additional weighting function and $Lq_j^{SR,SL}$ are LUIS corrections of “ q ” at the interface r_j (see Fig. 2, which are computed in the following manner:

$$\begin{aligned} Lq_j^{SR} &= \sum_{l=j-2}^{l=j} q_l \prod_{i \neq k, k=j-2}^{k=j} \frac{r_j - r_k^m}{r_i^m - r_k^m}, \quad \text{if } V_j \leq 0 \\ Lq_j^{SL} &= \sum_{l=j}^{l=j+2} q_l \prod_{i \neq k, k=j+2}^{k=j} \frac{r_j - r_k^m}{r_i^m - r_k^m}, \quad \text{if } V_j > 0. \end{aligned} \quad (16)$$

However, in order to maintain monotonicity of schemes, high order advection schemes must degenerate into lower ones close to shock fronts, which in turn

enhance the production of numerical entropy/diffusion. Therefore, in most of the test calculations presented here it was necessary to have $\xi > 1/2$ in order to damp overundershootings and enable convergence.

4. VERIFICATION TESTS

In this section we present results of various verification tests of the advection scheme using different energy formulations. Although the scheme can be applied to fluid-transport in multi-dimensions, the focus of the present study will be just to examine transport in one-dimension. Thus, the equations to be solved in this case are the continuity, radial momentum, internal and the total energy equations described in Eqs. (1)-(4).

The widely used hydrodynamical test in 1D is the one-dimensional relativistic shock tube problem (henceforth RSTP). The advantages of this test problem is that the obtained numerical solutions can be compared with the corresponding analytical solution with arbitrary large Lorentz factors.

For further details on the background of this test problem and the way the analytical solutions are obtained we refer the reader to (Marti and Müller 2003).

The RSTP is an initial value problem, in which the solution depends mainly on the initial conditions. The domain of calculations is divided into a right and left regions (see Fig. 2). In the left region $0 \leq x \leq x_c$: we set $P_L = 40/3$, $\rho_L = 10$ and in the right region $x_c < x$: we set $P_R = (2/3) \times 10^{-6}$, $\rho_R = 1$. The initial velocity is set to vanish everywhere.

Using the total energy formulation (TEF) we show in Figures (3-12) the profiles of the velocity and the corresponding Lorentz factor for different distributions of the initial conditions.

In Fig.3 we show the profiles of the velocity and Lorentz factor after 0.2 sec using the total energy formulation (see Eq. 2). To reduce computer time, the interval $[0.35 \leq x \leq 0.75]$ has been divided into 400 equally spaced cells, whereas 220 cells were used to cover the external intervals, where the variables continue to acquire their initial values. This grid distribution is set initially and remains fixed in time.

The advection scheme described in (Eq. 15) has been employed to achieve 3rd order spatial accuracy and the damped Crank-Nicolson method is used to achieve

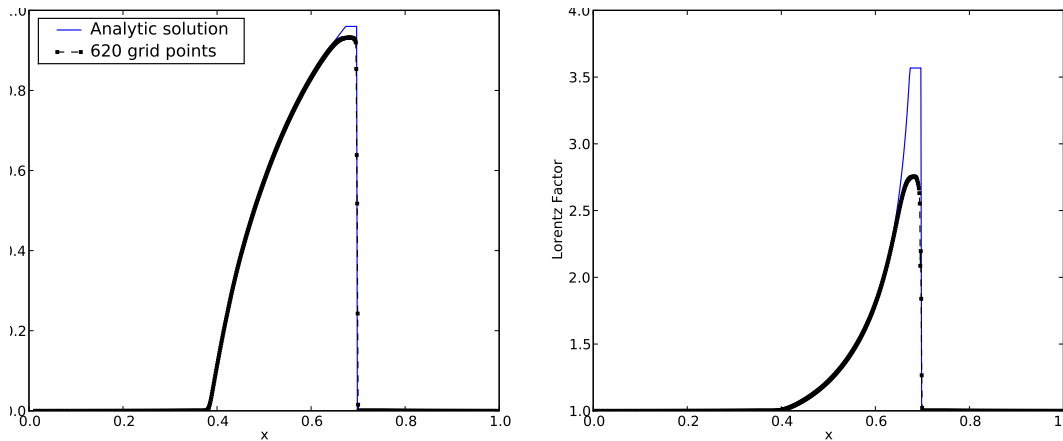


Figure 6. As in Fig (3), the profiles of V and u^t here have been obtained using the TEF method together with a heating source due to the artificial viscosity. An initial pressure $P_L = 10^2 P_{L0}$, $CFL = 0.4$ and a spatially third order accurate advection scheme in combination with two global iterations per time step have been used

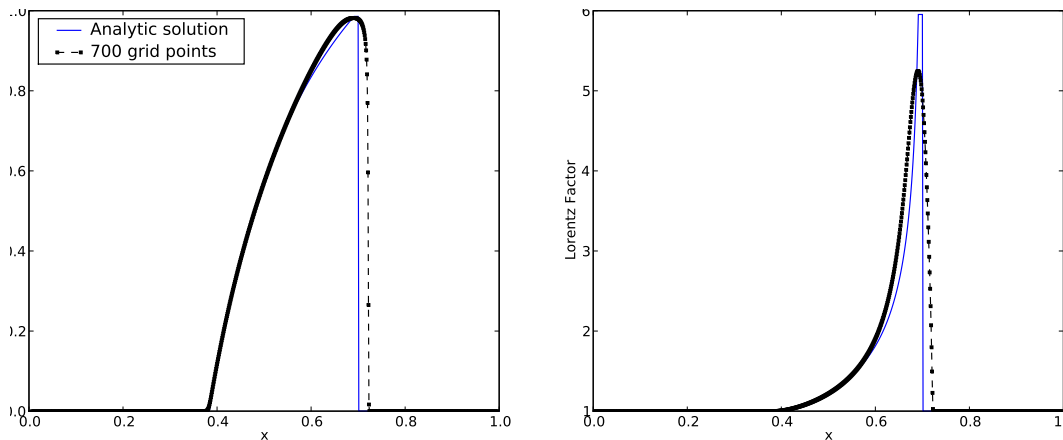


Figure 7. As in Fig (3), the profiles of V and u^t have been obtained using the pseudo-total energy formulation (PTEF, see Eq. 7), an initial pressure $P_L = 10^3 P_{L0}$, $CFL = 0.4$ and four global iterations per time step.

second order temporal accuracy (Hujeirat, Rannacher 2001). The time step size is set to have a maximum that corresponds to $CFL = 0.4$.

To test the robustness of the solution procedure, we have increased the P_L by a factor of 100, while the other variables remained unchanged. This increase of the pressure yields the Lorentz factor: $u^t \approx 3.6$ (Fig. 4). However, to enforce convergence, it was necessary to double the number of iteration per time step considerably. Comparing these results with those obtained using a double number of grid points and a halved time step-size, we could not observe a visibly significant improvement of the results.

From Figs. (5) and (6), we see that incorporating artificial viscosity and artificial heating while using the total energy formulation (TEF) has a similar effect as that of the normal numerical diffusion. In both cases the velocity at the shock front attains lower values than expected from the analytical solution.

We note that within the context of time-implicit solution methods, the total energy approach has a limited capability to accurately capture moving shocks at high Lorentz factors (Fig. 7). The reason is that, unlike the internal energy E_{in} , the kinetic energy E_{kin} increases with Lorentz factor as Γ^2 . As a consequence, the convergence

rate decreases with E_{in}/E_{kin} . In this case it is necessary to decrease both the time step size and the grid spacing in addition to allow an increase of the number of iteration per time step. The actual number of iteration per time step required to assure convergence is residual-dependent and in most cases cannot be determined a priori. Our test calculations with large gamma-factors showed a sharp increase of the actual number of iteration per time step (e.g., from 4 iteration for $\Gamma \approx 3.6$ to 12 for $\Gamma \approx 6$) or even a stagnation of the solution method.

On the other hand, our time-implicit solution method is found to be more robust if the internal energy formulation (IEF, see Fig. 2) is used. In Figures (8-12), the results of several test calculations are shown, which agree well with the analytical solutions. Moreover, the IEF method is numerically stable and the implicit solution procedure converges even when running the calculations with $CFL \geq 1$ (see Figs. 11 and 12).

The major draw back of the IEF is the necessity to fine-tune the coefficients of the artificial viscosity in order to obtain the correct Lorentz factor that fits well with the analytical solution. By fine-tuning we mean a posteriori adjustment of the numerical to the analytical solution by carefully fitting the artificial viscosity coefficient so to attain the best agreement between both.

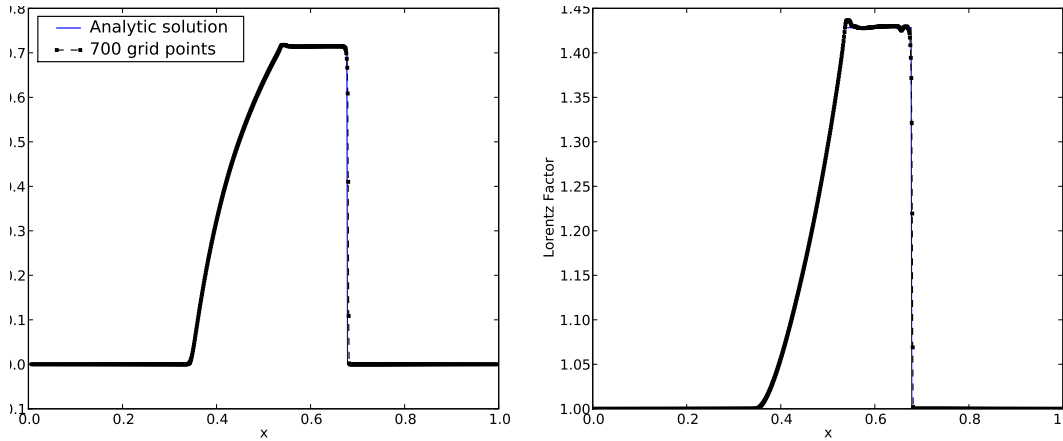


Figure 8. As in Fig (3): the profiles of V and u^t have been obtained using the internal energy formulation (IEF, see Eq. 3), the initial pressure $P_L = P_{L0}$, $CFL = 0.4$ and in combination with two global iterations per time step.

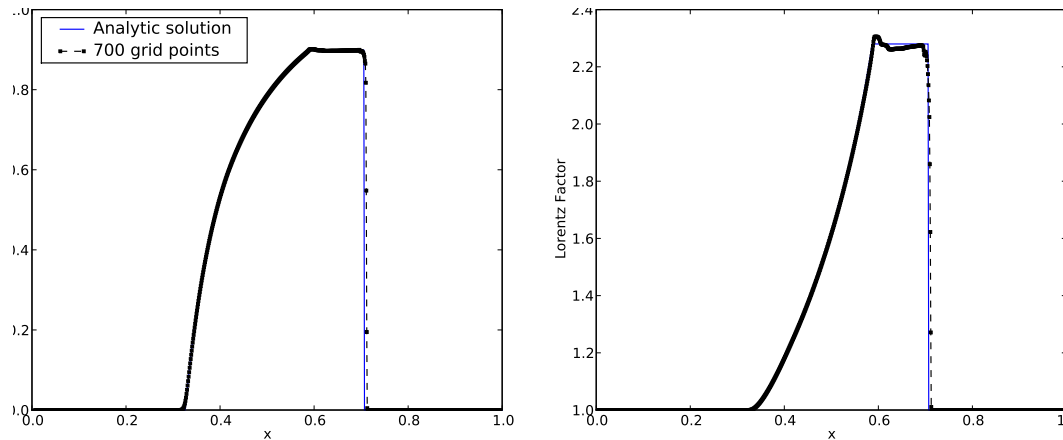


Figure 9. Similar to Fig (3), the profiles of V and u^t have been obtained using the IEF with the initial pressure $P_L = 10P_{L0}$ in combination with two global iterations per time step. The rest of variables remained as in Fig. (1) unchanged.

Moreover, the fine-tuning procedures must be repeated each time the ratio of the pressure P_L/P_R is changed. This is a consequence of the conversion of kinetic energy into heat at the shock fronts which cannot be determined a priori and uniquely by solely solving the internal energy equation.

Nevertheless, using the IEF, non-linear physical processes can be easily incorporated into the implicit solution procedure. Unlike in the TEF case, such processes are direct functions of the internal energy and therefore it is much easier to compute their entries and incorporate them into the corresponding Jacobian. This has the consequence that calculations can be performed also with $CFL \geq 1$, while still maintaining consistency with the original physical problem.

Finally, in Fig. (13) we show the profiles of V and u^t using the compact internal energy formulation (CIEF, Eq.(4) with high accuracies. The method is found to display overshooting and undershooting both at the contact discontinuity and the shock front, whose appearing was difficult to prevent through enlarging the number of grid points, decreasing the time step, enhancing the number of iteration per time step or even by activating the artificial viscosity. It should be noted here that since in the limit of large Lorentz factors, the CFL number depends weakly on

the sound speed (see Fig. 14), increasing the number of global iterations per time step has more significant effect on convergence than merely decreasing the time step size.

To examine the stability of the advection scheme at extremely high Lorentz factors, i.e., $\Gamma \geq 10$, we applied the solver to the relativistic planer shock reflection problem (RPSR), which has been comprehensively discussed by Alay et al. (1999).

The RPSR problem is based on simulating the collision of two relativistically, oppositely directed and equally fast moving cold plasmas. After they collide, an intermediate region of motionless, hot and dense matter is formed at the center.

The following initial conditions are used: $\rho_L = \rho_R = 1$, $\epsilon_L = \epsilon_R = 2.29 \times 10^{-5}$ and allow the plasmas to collide with $V_L = -V_R$ at the middle point, i.e., at $x=0.5$ in Fig (14). We then gradually increase V_R to reach almost the speed of light.

In Fig (14), the profiles of the density of the shocked motionless matter in the intermediate region, that have been obtained using different collisional speeds, are shown. As expected, the post-shock density in the intermediate region correlates with the collisional speed of the plasma. Although our results agree well with those reported by Alay et al. (1999) for $V < 0.999999$,

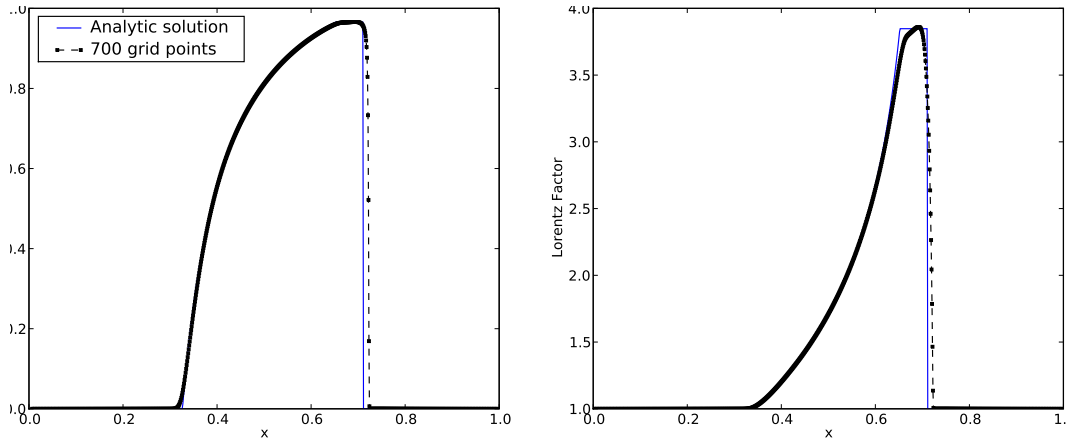


Figure 10. As in Fig (3), the profiles of V and u^t have been obtained after $\tau = 0.215$, using the IEF, an initial pressure $P_L = 10^2 P_{L0}$, $CFL = 1.5$ and four global iteration per time step

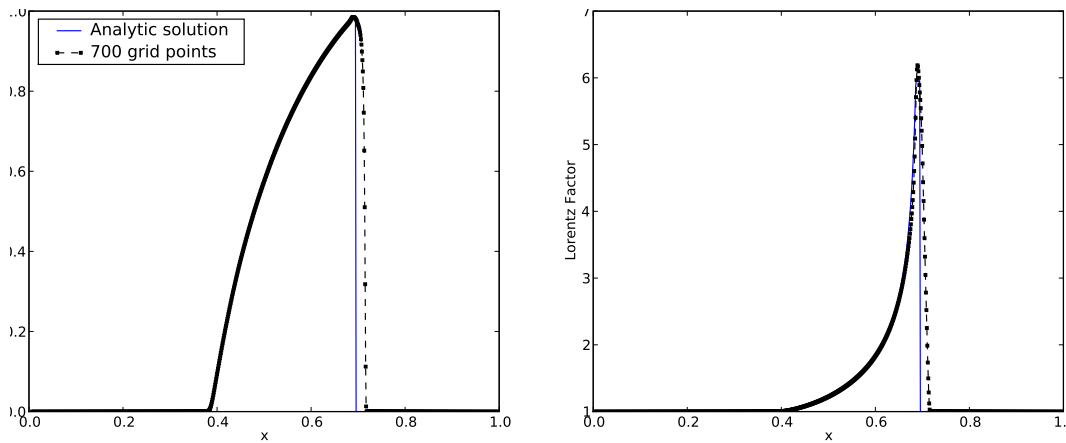


Figure 11. As in Fig (3), the profiles of V and u^t have been obtained using the IEF method, an initial pressure $P_L = 10^3 P_{L0}$, $CFL = 2$ in combination with five global iterations per time step.

our advection scheme seems to diverge for $V > 0.99999$. It shows some sort of sub-grid oscillations associated with under and overshootings both at the center as well as at the front of the reflected shock. We attribute this problem to the enhanced numerical errors in the evaluation of the Lorentz factor from the normalization condition as well as from the inverse non-linear transformation between the conservative and primitive variables. Our attempts in this regime to further optimize the shock capturing scheme or using other formulations of the normalization condition produced non-noticeable improvement to the results.

Nevertheless, the test calculations show that our numerical procedure presented here is robust and capable of dealing accurately with ultra-relativistic velocities that govern the fluid-motions in diverse astrophysical events, such as in quasars or jetted Gamma-ray bursts. However, testing the advection scheme for velocities corresponding to $\Gamma > 1000$ is physically irrelevant, as the fluid-description of plasmas breaks down.

5. SUMMARY AND CONCLUSIONS

In this paper we have presented a numerical scheme for time-implicit modeling of relativistic shocks with high Lorentz factors. The results of several verification tests

using the internal energy (IEF), the total energy (TEF) and pseudo-total energy (PTEF) formulations have been presented as well.

To be stressed here that time-explicit methods are efficient and best suited for modeling strongly time-dependent flow-problems much more than their implicit counterparts. This is to be attributed to the fact that in implicit methods the coefficients of preconditioning matrix should be evaluated and inverted several times per time step, in order to recover the non-linearities accurately. Furthermore, when modeling moving shocks or strongly time-dependent flows, a time step-size which corresponds to $CFL < 1$ should be used to assure accurate capturing of the temporal behaviour of the flows in critical regions.

On the other hand, implicit solvers are advantageous over explicit solution methods when dealing with reacting flows with physical processes operating on shorter or longer time scales compared to the dynamical one or when the flows are viscous-dissipative. Therefore, our attempt in this paper is to enlarge the range of applications of the solver GR-I-RMHD to cover the regime of moving shocks at relatively high Lorentz factors.

Our test calculations show that TEF is most suited for modeling the propagation of shocks with low to moderate Lorentz factors, though with low CFL numbers, hence

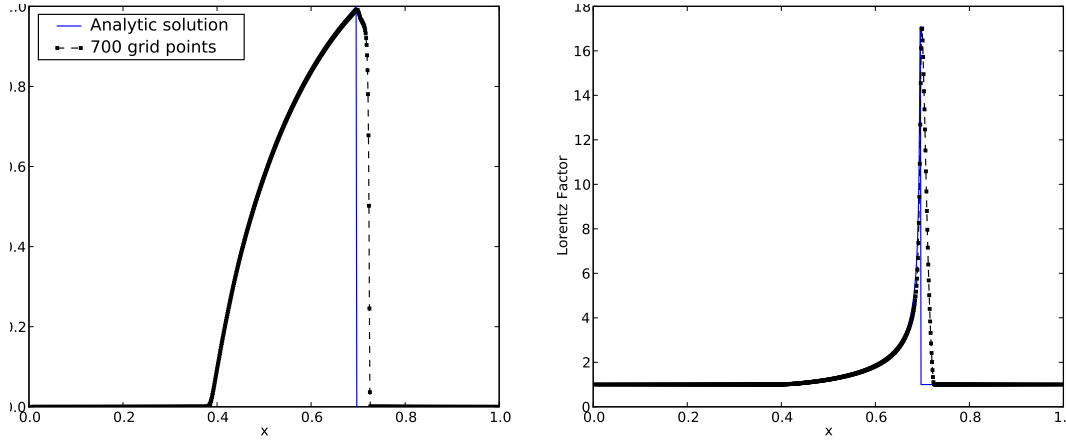


Figure 12. As in Fig (3), the profiles of V and u^t have been obtained using the IEF method, an initial pressure $P_L = 10^5 P_{L0}$, $CFL = 4$ in combination with seven global iterations per time step.

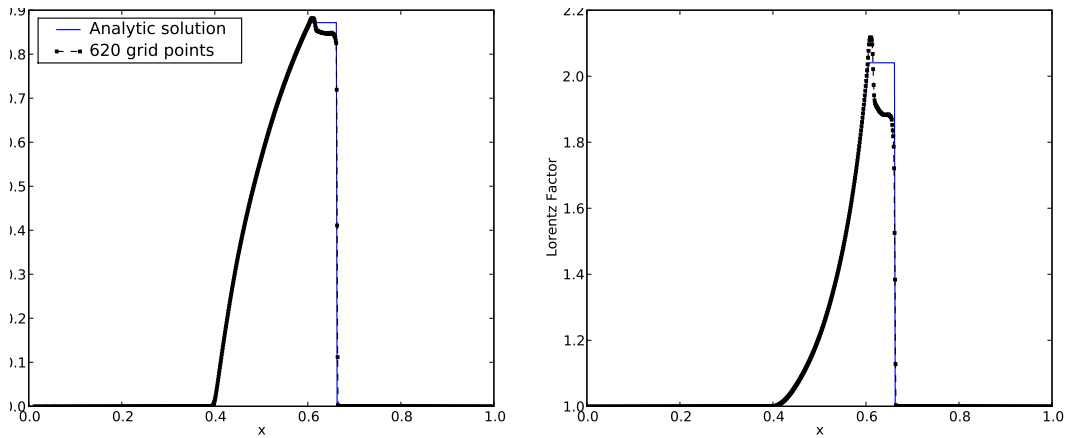


Figure 13. As in Fig (3), the profiles of V and u^t are shown after $\tau = 0.175$. These have been obtained using the compact internal energy formulation (CIEF, see Eq. 4), initial pressure $P_L = 10P_{L0}$ in combination with two global iterations per time step

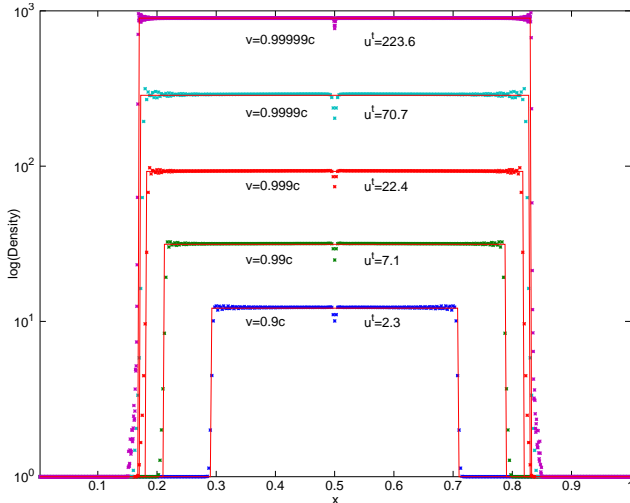


Figure 14. Shock reflection problem: various density profiles resulting from different collisional speeds (v in units of the speed of light) versus the distance from the collisional center $x=0$, using 400 grid points and $CFL=0.3$ after the elapsed time $t = 1$. The corresponding Lorentz factor u^t is assigned to each profile.

more suitable for time-explicit solution methods.

On the other hand, although the PTEF is similar to the TEF, it was found that a larger number of iterations per time step was required to maintain convergence.

Using the IEF however, it has been verified that the implicit solution procedure converges relatively fast even for Lorentz factors $u^t \gg 1$ and the $CFL \geq 1$.

It should be stressed here that the IEF has a major drawback, as it requires a fine-tuned parameters of the artificial viscosity to obtain correct Lorentz factors at the shock fronts. On the other hand, when modeling astrophysical plasmas, the IEF is favorable over TEF, as cooling and heating processes are generally direct functions of the internal energy, and so it is easier to linearize and construct the coefficients to be incorporated into the Jacobian.

Furthermore, turbulence is an intrinsic property of most astrophysical fluid flows. The artificial viscosity in such flows is redundant when turbulent diffusion is taken into account, therefore relaxing the fine-tuning problem of the artificial viscosity. In the case of ideal flows (; non-viscous, magnetic and radiative non-diffusive flows), the solution procedure should run similar to the

those adopted in the present test calculations together with a re-start option in combination with a careful data-storage strategy. Having started the calculations with an enhanced artificial viscosity, the calculation can then be re-started after a certain elapsed time while gradually decreasing the viscosity coefficient till the optimal value is reached.

Nonetheless a fine-tuned artificial viscosity may turn out to be necessary also for numerical schemes using the total energy formulation, in particular when shock-formation in the vicinity of relativistic objects is to be modeled. In this case the ratio of the internal to the total energy can be as low as δt or even smaller. Using highly accurate non-diffuse numerical advection schemes may easily lead to over/under-shootings of the values of the conservative variables at the shock front⁵ that give rise to negative temperatures, hence to a stagnation of the solution procedure.

We note that the phenomenon of shock propagation with high Lorentz factors has been poorly studied numerically, despite the availability of relatively large number of relativistic explicit codes. Most of these numerical studies rely on using the TEF-method and the results obtained are indeed highly accurate (see for example Hawley et al. 1984; Alay et al. 1999; De Villiers, Hawley 2003; Gammie et al. 2003; Anninos, Fragile 2003; De Colle et al. 2011). On the other hand, to our knowledge PLUTO is the only solver that has been verified to accurately capture shock fronts propagating with high Lorentz factors, i.e., $\Gamma > 5$ (Mignone et al. 2007). For $P_L = 10^3 P_R$, PLUTO results agree well with our results displayed in Fig.11. For much higher Γ -factors we strongly recommend using an implicit method in combination with the internal energy formulation.

While simulating the propagation of ultra-relativistic shock-fronts in 1D using implicit methods is to date a feasible task on personal computers, the situation in 2D may still be different. For example, assume we want to estimate the computational costs associated with modeling the motion of 2D-curved relativistic shocks in the vicinity of a black hole (e.g., with $\Gamma = 17$ as in Fig.12). The computational domain should consist of approximately $N \times N = 1000 \times 1000$ non-uniformly distributed grid points. The corresponding pre-conditioner would have a band width: $m_{bw} \approx 15$. The computational costs per iteration would roughly be of the order $CC \approx m_{bw} \times N^2$. Taking into account that approximately 10 iterations per time step are needed and that a total number of about 10^5 time steps are required in order to recover several dynamical time scales, we end up with approximately 10^{13} arithmetic operations. This number, however, may be modified considerably when the overhead operations are taken into account. It may even increase by additional seven orders of magnitude, if the third spatial dimension is included or when magnetic fields and/or radiation are taken into account.

Therefore, carrying out such calculations is indeed a

challenging endeavor.

Concerning the evaluation of the Lorentz factor, we find that irrespective of the method used for solving the energy equation, the Lorentz factor is found to be best computed from the normalization condition in which the transport velocities and momenta are used.

We have also presented a modified MUSCL advection scheme of third order spatial accuracy, which has been constructed to enable accurate capturing of relativistically moving shocks. The accuracy of the scheme can be further enhanced by incorporating the Lagrangian Upwind Interpolation Scheme (LUIS).

Nevertheless, for saving computer time, we recommend using the LUIS scheme when strongly time-dependent flows with prominent shock fronts are to be simulated.

Noting that the appropriate parameters of the artificial viscosity cannot be determined a priori, obtaining the correct Lorentz factor may turn out to be a difficult task. In the case of standing shocks, the hierarchical solution scenario in combination with the defect-correction iteration procedure (Hujeirat 2005) can be employed to gradual-enhance the accuracies of the scheme and obtain the correct Lorentz factors at the shock fronts.

In a forthcoming paper, we intend to study the formation of strong shocks in curved spacetime near the surface of ultra-compact neutron stars.

Acknowledgment SF thanks the SNF for the financial support.

REFERENCES

- Biretta, J.A., 1999, AAS, 195, 5401
 Marscher, A.P., 2006, AIPC, 856, 1
 Aloy, M.-A., Ibanez, J.M., Mart, J.M., Müller, E., 1999, ApJS, 122, 151 (GENESIS)
 Anninos, P., Fragile, P. C., 2003, ApJ. Suppl. Ser., 144, Iss. 2, 243-257
 Del Zanna, L., Bucciantini, N., 2002, A&A, 390, 1177-1186
 Del Zanna, L., Zanotti, O., et al., 2007, A&A, 473, 11
 De Villiers, J.-P., Hawley, J.F., 2003, ApJ, 589, 458
 Fender, R., Koerding, E., Belloni, T., et al. 2007, astro-ph, 0706.3838
 De Colle, F., Granot, J., Lopez-Camara, D., Ramirez-Ruiz, E., 2011, astro-ph, 1111.6890
 Font, J.A., Miller, M., Suen, W., Tobias, M., 2000, Phys. Rev. D, 61, 044011
 Font, J.A., 2003, LRR, 6, 4
 Gammie, C. F., McKinney, J. C., Tóth, G., 2003, ApJ, 589, 444-457 (HARM)
 Hawley, J.F., Smarr, L.L., Wilson, J.R., 1984, ApJS, 55, 211
 Hirsch, C., 1988, "Numerical Computation of Internal and External Flows", Vol. I, II, John Wiley & Sons, New York
 Hujeirat, A., Rannacher, R., 2001, New Ast. Reviews, 45, 425
 Hujeirat, A., Livio, M., Camenzind, M., Burkert, A., 2003, A&A, 408, 415
 Hujeirat, A., 2005, CoPhC, 168, 1
 Hujeirat, A., Camenzind, M., Keil, B.W., 2008, New Astronomy, 13, 436
 Hujeirat, A., Thielemann, F.-K., 2009, A&A, 496, 609
 Hawley, J. F., Smarr, L. L., Wilson, J. R., 1984a, ApJ, 277, 296-311
 Hawley, J. F., Smarr, L. L., Wilson, J. R., 1984b, ApJS, 55, 211-246
 Koide, S., Shibata K., Kudoh, T., 1999, ApJ, 522, 727
 Komissarov, S.S., 2004, MNRAS, 350, 1431

⁵ It should be noted that most highly accurate advection schemes generally violate the monotonicity condition in such critical regions (LeVeque 1990).

LeVeque, R.J., 1990, "Numerical Methods for Conservation Laws", Birkhauser-Verlag, Basel
Livio, M., 2004, BaltA, 13, 273L
Marti, J.M., Müller, E., 2003, LRR, 6, 7
Mignone, A., Bodo, G., Massaglia, et al., 2007, ApJS, 170, 228-242 (PLUTO)

Mizuno, Y., Nishikawa, J.-I., et al., 2006, astro-ph/0609004 (RAISHIN)
Piran, T., 2005, RvMP, 76, 1143
Sikora, M., Begelman, M.C., Rees, M.J., 1994, ApJ, 421, 153
Zhang, W., MacFadyen, A.I., 2006, ApJS, 164, 255